THE ASTROPHYSICAL JOURNAL, 436:L5–L8, 1994 November 20

ASCA MEASUREMENTS OF THE GRAIN-SCATTERED X-RAY HALOS OF ECLIPSING MASSIVE X-RAY BINARIES: VELA X-1 AND CENTAURUS X-3

JONATHAN W. WOO AND GEORGE W. CLARK[1]
Center for Space Research, Massachusetts Institute of Technology, Cambridge, MA 02139
CHARLES S. R. DAY
Laboratory for High Energy Astrophysics, NASA/Goddard Space Flight Center, Greenbelt, MD 20771
FUMIAKI NAGASE
The Institute of Space and Astronautical Science, 3-1-1 Yoshinodai, Sagamihara, Kanagawa 229, Japan
AND
TOSHIAKI TAKESHIMA
Institute of Physical and Chemical Research, 2-1 Hirosawa, Wako, Saitama 351-01, Japan
Received 1994 June 20; accepted 1994 August 31

ABSTRACT

We have measured the decaying dust-scattered X-ray halo of Cen X-3 during its binary eclipse with the *ASCA* solid-state imaging spectrometer (SIS). The surface brightness profile (SBP) of the image in the low-energy band (0.5–3 keV) lies substantially above the point-spread function (PSF) of the X-ray telescope, while the SBP in the high-energy band (5–10 keV) exhibits no significant deviation. By contrast, the SBPs of Vela X-1 during its eclipse are consistent with the PSF in both the low- and high-energy bands—strong evidence that a dust halo is indeed present in Cen X-3. Accordingly, we modeled the SBP of Cen X-3 taken from six consecutive time segments under the principal assumptions that the dust is distributed uniformly along a segment of the line of sight, the grains have a power-law size distribution, and the low-energy source flux was the same function of orbital phase before as during our observation. The best-fit set of parameters included a grain density value of 1.3 g cm^{-3}, substantially less than the density of "astronomical silicate." This result supports the idea that interstellar grains are "fluffy" aggregates of smaller solid particles. We attribute the failure to detect a halo of Vela X-1 during its eclipse phase to extended strong circumsource absorption that probably occurred before the eclipse and allowed the halo to decay away before the observation began.

Subject headings: binaries: eclipsing — dust: extinction — pulsars: individual (Vela X-1, Centaurus X-3) — X-rays: stars

1. INTRODUCTION

An X-ray source observed through the interstellar medium has a "halo" of X-rays scattered by dust grains lying near the line of sight (Overbeck 1965). The intensity and radial distribution of the scattered X-rays depend on the energy of the X-rays and on the properties of the interstellar grains (i.e., density, composition, size, and spatial distribution). Thus, the X-ray halos of point sources can be used as diagnostics of interstellar grains (Mathis & Lee 1991 and references therein). As Xu, McCray, & Kelley (1986) pointed out, an eclipsing X-ray binary offers a unique advantage for the study of interstellar grains; when the X-ray star goes into eclipse, the X-ray intensity of the direct component decreases abruptly to about 1% or 2% of its uneclipsed value (the residual direct intensity is due primarily to Compton scattering by circumsource matter) while the halo decays gradually owing to relative delays in the travel times of the scattered X-rays. Therefore, during an eclipse that is preceded by a period of high X-ray intensity, one can expect to observe a decaying halo with a minimum of interference from X-rays coming directly from the occulted source.

This *Letter* is concerned with the X-ray halo phenomena of Cen X-3 and Vela X-1 as revealed by an analysis of *ASCA* images recorded both in and out of their eclipses. Cen X-3 and Vela X-1 are massive binary X-ray pulsars with orbital periods of 2.08 days and 8.96 days, respectively. Their properties have been reviewed recently by Nagase (1989). Since the optical counterparts of both X-ray sources show strong extinction (E_{B-V} is 1.4 for Cen X-3 and 0.7 for Vela X-1), both sources are expected to have substantial X-ray halos during any period of sustained X-ray brightness.

A decaying X-ray halo of Cen X-3 was observed during eclipse with *EXOSAT* by Day & Tennant (1991). Lewis et al. (1992) found no evidence of a soft time-dependent grain-scattered component in the eclipse spectrum of Vela X-1 observed by *Ginga*. They suggested that the grain-scattered X-ray halo had decayed away during the highly absorbed pre-eclipse phase. Clark, Woo, & Nagase (1994) extracted the grain-scattered X-ray halo component from the spatially unresolved *Ginga* observation of 4U 1538−52 during its eclipse phase. They concluded that the X-ray scattering efficiency of interstellar grains is less than that expected for solid grains of "astronomical silicate" and suggested that the result supports the idea (Mathis & Whiffen 1989) that interstellar grains are "fluffy" aggregates with an average bulk density less than that of their constituent particles. Predehl & Schmitt (1994) also found evidence of a scattering efficiency less than that of solid grains in their study of X-ray halos in 25 point sources and four supernova remnants based on *ROSAT* observations.

Here we describe our analysis of the surface brightness profiles (SBPs) of images of Cen X-3 and Vela X-1 recorded by

[1] Department of Physics, Massachusetts Institute of Technology, Cambridge, MA 02139.

ASCA and our interpretation of the observed halo phenomena of Cen X-3 in terms of the properties of interstellar grains.

2. OBSERVATIONS AND DATA ANALYSIS

The observations were made with the solid-state imaging spectrometer (SIS) of the *ASCA* X-ray observatory (Tanaka, Inoue, & Holt 1994). Cen X-3 was observed on 1993 June 24 for 1 day over its binary orbital phase interval between -0.3 and 0.2. Vela X-1 was observed on 1993 June 25–26 and July 5 for ~ 2.5 days over its binary orbital phase interval between -0.15 and 0.15. The SIS has a 22′ square field of view and is sensitive in the energy range from 0.3 to 12 keV. The point-spread function (PSF) of SIS images is determined by the telescope with no significant additional spread introduced by the SIS itself.

Figure 1*a* shows the light curves of Vela X-1 and Cen X-3. In both cases the X-ray eclipses occur within the orbital phase intervals between -0.1 and 0.1, and the count rates during the eclipses are small but significantly above the sky background level ($\sim 10^{-4}$ counts s^{-1}). Both sources show extended pre-eclipse low states before the eclipses; it is not clear when the preeclipse low state of Vela X-1 began, but that of Cen X-3 began near $\phi_{\rm orb} \sim -0.25$.

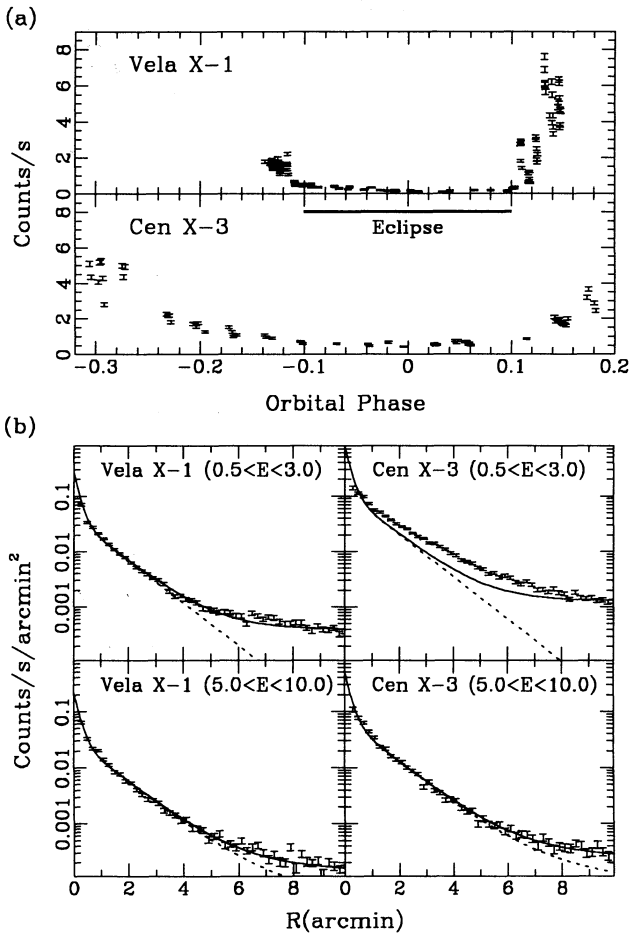

FIG. 1.—(*a*) X-ray light curves of Vela X-1 and Cen X-3. The total count rates of one chip (S0C1) in 256 s integration times are plotted against orbital phases. (*b*) SBPs of Vela X-1 and Cen X-3 in two energy bands: $0.5 < E < 3.0$ keV and $5.0 < E < 10.0$ keV. The solid lines represent the sums of the PSF plus a constant background fitted within $R < 1'$ and $8' < R < 10'$. The dashed lines represent the PSF component only.

We constructed SBPs of the Cen X-3 and Vela X-1 images in two energy bands from data recorded in and out of the eclipse. We then compared the SBPs with the telescope PSF as represented by the following expressions for surface brightness $S(R)$ as a function of the angular distance R from the center in arcminutes:

$$S(R) = \begin{cases} N[0.6457 \exp(-R/0.1867) + 0.1033 \exp(-R/1.1505)], \\ \qquad 0.5 < E < 3.0 \text{ keV}; \\ N[0.5757 \exp(-R/0.1867) + 0.0943 \exp(-R/1.1505) \\ \qquad + 0.00068 \exp(-R/6.9)], \\ \qquad 5.0 < E < 10.0 \text{ keV}. \end{cases} \quad (1)$$

These functions were fitted to the SBPs of the Cen X-3 and Vela X-1 images by adjusting the normalization factor N and a constant background to match the data within 1′ of the center and beyond 8′. As shown in Figure 1*b*, the Vela X-1 SBPs in both the low- and high-energy bands agree well with the PSFs plus a constant background as indicated by the solid lines. The X-ray background level becomes significant for $R < 4'$ and has fitted values of $\sim 4 \times 10^{-4}$ counts s^{-1} arcmin^{-2} for the low-energy band ($0.5 < E < 3.0$ keV) and $\sim 1 \times 10^{-4}$ counts s^{-1} arcmin^{-2} for the high-energy band ($5.0 < E < 10.0$ keV). The fitted PSF (without background) is indicated by the dashed lines. The same background levels are found when the out-of-eclipse SBPs are fitted in the same manner.

The high-energy SBP of Cen X-3 in the eclipse phase (Fig. 1*b*) is also well represented by the high-energy PSF and a constant background level, which in this case is $\sim 1.5 \times 10^{-4}$ counts s^{-1} arcmin^{-2}. This proves that the contribution of errors in attitude determinations to the SBPs was not larger in the case of Cen X-3 than in the case of Vela X-1. However, the low-energy SBP of Cen X-3 cannot be fitted by the low-energy PSF plus a constant background. We believe that (1) the excess of the Cen X-3 low-energy SBP above the PSF, which fits the Vela X-1 data, and (2) the contrast between the high- and low-energy SBPs of Cen X-3 itself are certain evidence of a grain-scattered halo in Cen X-3. Since the halo contributes to the SBP within $R < 1'$ where the PSF is fitted by adjustment of the normalization factor, the solid lines in Figure 1*b* represent upper limits to the contribution of core and background to the SBPs, and the difference between the solid line and the data is, correspondingly, a lower limit on the halo intensity. The background level, determined from the data beyond 8′, is $\sim 1.3 \times 10^{-3}$ counts s^{-1} arcmin^{-2}.

We focus now on an analysis of the Cen X-3 halo. In the ideal case of a source with steady intensity and no eclipse, the ratio of X-ray scattering to optical extinction can be characterized by the quantity

$$R_{\rm XV} = (E/1 \text{ keV})^2 (I_g/I) A_V^{-1} \text{ mag}^{-1}, \quad (2)$$

where the ratio I_g/I is the fractional halo intensity at energy E (see Clark, Woo, & Nagase 1994). In principle $R_{\rm XV}$ is determined by the properties of the grains. To set lower limits on $R_{\rm XV}$ we constructed average SBPs in two narrow energy bands ($1 < E < 2$ keV and $2 < E < 3$ keV) for the six time intervals labeled A to F in Figure 2*a*. We fitted the low-energy PSF to the core ($R < 1'$) and tail ($8' < R < 10'$) regions of each SBP by adjusting the normalization factor N and a background rate which was $\sim 8 \times 10^{-4}$ counts s^{-1} arcmin^{-2} for $1 < E < 2$ keV

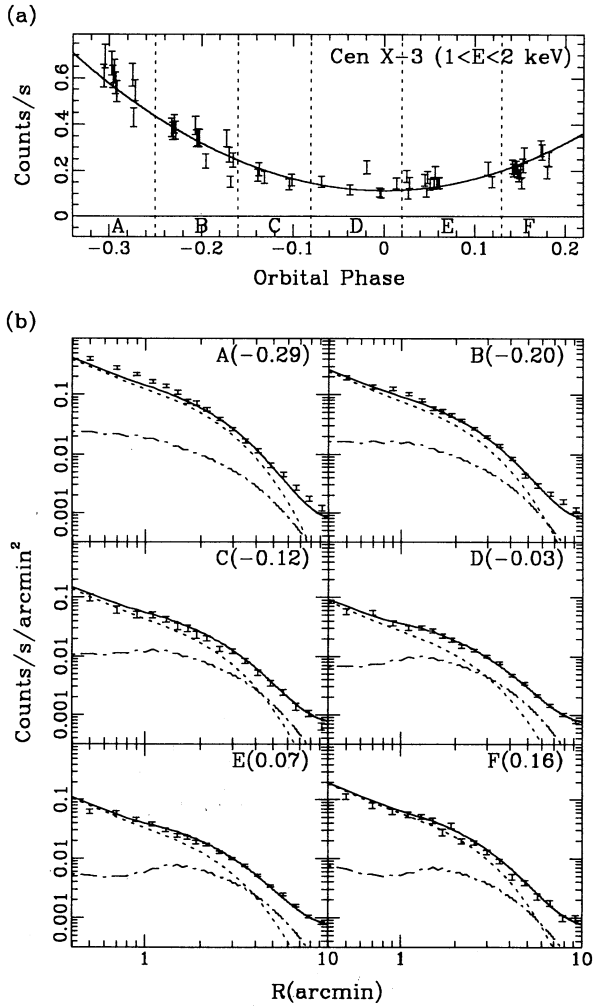

FIG. 2.—(*a*) The X-ray light curve of Cen X-3 for $1 < E < 2$ keV. The solid line represents a quadratic fit for $-0.3 < \phi < 0.3$. The dotted vertical lines separate six time intervals as marked with letters A–F. (*b*) The six SBPs of Cen X-3 in the six time intervals marked in (*a*) for $1 < E < 2$ keV. The numbers in the upper right-hand corners are the middle orbital phases for each SBP. The solid lines, representing the fitted SBPs, are the sums of the core component (*dotted line*), halo component (*dot-dashed line*), and a constant background ($\sim 6 \times 10^{-4}$ counts s^{-1} arcmin^{-2}).

and $\sim 2 \times 10^{-4}$ counts s^{-1} arcmin^{-2} for $2 < E < 3$ keV. In each time segment we estimated the halo intensity as the difference between the SBP and the fitted PSF. (In the case of segment A there was no significant difference, which we attribute to the inability of the instrument to resolve a relatively small halo component from the direct source component.) We then substituted for I_g/I in equation (2) the ratio of this halo intensity estimate for each of segments B to F to the core intensity in segment A as represented by the fitted PSF for that segment. For the effective energy E of the detected X-rays we substituted the values 1.5 keV and 2.5 keV for the two energy ranges, respectively. Since some halo intensity is always present within $R = 1'$, the halo intensities are underestimated in this procedure, and the core intensity is overestimated. Moreover, the effective core intensity for generating the halo decreases after the eclipse begins. Thus, the quantities derived in this way are lower limits on the value of R_{XV}. The results are summarized in Table 1.

TABLE 1

DERIVED VALUES OF R_{XV}

Time	R_{XV} (1 σ) (1–2 keV)	R_{XV} (1 σ) (2–3 keV)
B	0.077 (0.006)	0.086 (0.014)
C	0.050 (0.006)	0.063 (0.013)
D	0.052 (0.003)	0.084 (0.006)
E	0.051 (0.002)	0.061 (0.006)
F	0.075 (0.005)	0.056 (0.014)

We next place constraints on a grain model by fitting calculated SBPs simultaneously to the six average SBPs for the energy range $1 < E < 2$ keV, taking account of the variability of the halo intensity. For this purpose we call $I_h(\theta, t)$ the surface brightness of the halo at angle θ and time t due to single scattering. Adapting a formula of Mathis & Lee (1991) for the angular spread of the halo of a steady source at distance D to the present condition of an eclipsed source with a decaying halo, we obtain the formula

$$I_h(\theta, t) = N_H \int dE \int n(a)da \int \frac{f(x)}{(1-x)^2} \frac{d\sigma_{sc}(a, E, \theta, x)}{d\Omega} \times I[E, t'(x)]dx , \quad (3)$$

where N_H is the total column density of hydrogen atoms, $I(E, t')dE$ is the total intensity of photons with energy in the range from E to $E + dE$ at the earlier time $t' = t - (D/2c)(x\theta^2)/(1 - x)$ (Trümper & Schönfelder 1973), $n(a)da$ is the number of grains (assumed to be homogeneous and spherical) per hydrogen atom with radii in the range from a to $a + da$, x is the fractional distance of the scattering site between the observer and the X-ray source, and $f(x)$ is the density of hydrogen atoms at position xD along the line of sight relative to the average density. In the Rayleigh-Gans approximation,

$$\frac{d\sigma_{sc}(\theta)}{d\Omega} = (1.1 \text{ cm}^2 \text{ sr}^{-1}) \left(\frac{2Z}{M}\right)^2 \left(\frac{\rho}{3 \text{ g cm}^{-3}}\right)^2 \times a(\mu\text{m})^6 \left[\frac{F(E)}{Z}\right]^2 \Phi^2(\theta) , \quad (4)$$

where Z is the mean atomic charge, M is the mean molecular weight, ρ is the mass density, $F(E)$ is the atomic scattering factor given by Henke (1981), and Φ is the "form" factor which is well approximated (Mauche & Gorenstein 1986) by a Gaussian,

$$\Phi_G^2(\theta) = \exp\left[-0.4575E(\text{keV})^2 a(\mu\text{m})^2 \theta(\text{arcmin})^2/(1-x)^2\right] . \quad (5)$$

We call $I_c(\phi)$ the core intensity at the binary orbital phase ϕ and represent it as a quadratic function $I_c(\phi = 0.5)(0.114 + 5.54\phi^2)$ in the phase interval $-0.4 < \phi < 0.4$, and as a constant function $I_c(\phi = 0.5)$ for $0.4 < \phi < 0.6$. The quadratic function was derived from a fit to the light curve (Fig. 2*a*) which was constructed from X-ray events in the energy range $1 < E < 2$ keV within 1′ of the image center. This light curve is symmetric about the eclipse center while the light curve for events of all energy (Fig. 1*a*) is significantly asymmetric, being substantially higher at $\phi = +0.2$ than at $\phi = -0.2$. We suggest that this difference is due to blockage of the direct soft X-rays from the neutron star by absorption in the accretion

TABLE 2

DERIVED PARAMETERS FROM SIMULTANEOUS FIT OF HALO MODEL TO SIX SURFACE BRIGHTNESS PROFILES OF CENTAURUS X-3 THROUGH AN ECLIPSE

Parameter	Value (1 σ)
I_c (counts s^{-1})	5.08 (0.04)
I_{bg} (10^{-4} counts s^{-1} arcmin^{-2})	6.59 (0.12)
x_{min}	0.052 (0.005)
x_{max}	0.717 (0.005)
f_ρ	0.43[a] (0.01)
χ_ν^2 (283 degrees of freedom)	1.66

[a] 0.67 if we assume $I_c(0.3 < \phi < 0.7) = I_c(\phi = 0.3)$ instead of $I_c(0.4 < \phi < 0.6) = I_c(\phi = 0.4)$.

disk, leaving only the albedo X-rays scattered from the atmosphere of the companion star. The observed gradual and symmetric variation of the count rate as a function of the orbital phase is similar to the variation of albedo intensity calculated by Haberl (1991) and Clark et al. (1994). Consistent with this idea is the fact that the spectrum of X-rays detected in time interval A appears to consist of a highly absorbed ($N_H > 10^{23}$ H atoms cm^{-2}) hard component and a separate soft component.

Lacking data from earlier times, we assumed that the core intensity had been varying periodically with orbital phase according to the above constant-plus-quadratic function, so that the implicit integration over time in equation (3) could be extended into the past. We then added the X-ray halo component calculated according to equation (3) and a constant diffuse X-ray background intensity I_{bg} to the core component distributed according to the PSF. We assumed that the size distribution of the grains was a power law with an index of -3.5 between 0.005 μm and 0.25 μm (Mathis, Rumpl, & Nordsieck 1977), and the density of grains was uniform between $x = x_{min}$ and $x = x_{max}$. We assumed $D = 6$ kpc. We set $2Z/M = 1$ and $F(E)/Z = 1$, which are good approximations for silicates, graphite, and ice. We allowed for possible "fluffiness" of the grains by setting $\rho = 3f_\rho$ g cm^{-3}. Thus, in the fitting calculation we had five adjustable parameters: $I_c(\phi = 0.5)$, I_{bg}, x_{min}, x_{max}, and f_ρ. The fitted parameters are listed in Table 2 together with statistical errors that are the deviations which increase the χ^2 of the fit by unity. The fitted contributions to the SBP of the core and halo components and their sum are shown as separate curves in Figure 2*b*.

We note that the fitted halo component behaves during the eclipse as one expects, namely, it dominates the SBP in the tail, it decays more rapidly at the center than in the tail, and it begins to recover after the eclipse.

3. DISCUSSION

That the SBP conforms to the PSF at high energies but deviates at low energies is clear evidence of an X-ray halo in Cen X-3 with a spectrum softened by E^{-2} relative to the spectrum of the direct component, as expected from the theory of grain scattering (van der Hulst 1957). The Cen X-3 halo has also been detected in *ROSAT* data (C. Mauche, private communication). Since Vela X-1 is much closer ($\sim$2 kpc) than Cen X-3 ($\sim$6 kpc) and, in addition, exhibits strong and extended preeclipse circumsource absorption (see Lewis et al. 1992), we conclude that most of its X-ray halo decayed away before the start of our observation.

All the lower limits on R_{XV} shown in Table 1 are consistent with the value 0.087 mag^{-1} derived from *ROSAT* observations of X-ray halos around 25 point sources and four supernova remnants (Predehl & Schmitt 1994). The theoretical values of R_{XV} are 0.22 and 0.11 mag^{-1} for solid grains of "astronomical silicate" and a mixture of graphite and astronomical silicate, respectively. As pointed out by Clark et al. (1994), the X-ray scattering efficiency of grains of a given chemical composition and size decreases more rapidly with density than the optical extinction efficiency. Thus, the R_{XV} values of grains made of these materials would be smaller if they are "fluffy" aggregates of smaller solid particles. Furthermore, our global fit of computed SBPs to the *ASCA* images of Cen X-3 by adjustment of the density of the grain model yields a value of the density approximately half that of solid "astronomical silicate." Thus, the present results, together with those of Clark et al. (1994) and Predehl & Schmitt (1994), support the idea (Mathis & Whiffen 1989) that interstellar grains are "fluffy" aggregates of smaller solid particles.

REFERENCES

Clark, G. W., Woo, J. W., & Nagase, F. 1994, ApJ, 422, 336
Day, C. S. R., & Tennant, A. F. 1991, MNRAS, 251, 76
Haberl, F. 1991, A&A, 252, 272
Henke, B. L. 1981, in Low Energy X-Ray Diagnostics, ed. D. T. Attwood & B. L. Henke (New York: AIP), 146
Lewis, W., Rappaport, S., Levine, A., & Nagase, F. 1992, ApJ, 389, 665
Mathis, J. S., & Lee, C. W. 1991, ApJ, 376, 490
Mathis, J. S., Rumpl, W., & Nordsieck, K. H. 1977, ApJ, 217, 425
Mathis, J. S., & Whiffen, G. 1989, ApJ, 341, 808
Mauche, C. W., & Gorenstein, P. 1986, ApJ, 302, 371
Nagase, F. 1989, PASJ, 41, 1
Overbeck, J. 1965, ApJ, 141, 864
Predehl, P., & Schmitt, J. H. M. M. 1994, A&A, in press
Tanaka, Y., Inoue, H., & Holt, S. S. 1994, PASJ, 46, L37
Trümper, J., & Schönfelder, V. 1973, A&A, 25, 445
van der Hulst, H. C. 1981, Light Scattering by Small Particles (New York: Dover)
Xu, Y., McCray, R., & Kelley, R. 1986, Nature, 319, 652